JOURNAL OF NANO- AND ELECTRONIC PHYSICS
Vol. **18** No 5, 05013(5pp) (2026)

ЖУРНАЛ НАНО- ТА ЕЛЕКТРОННОЇ ФІЗИКИ
Том **18** № 5, 05013(5cc) (2026)

OPEN ACCESS

REGULAR ARTICLE

Structural, Optical, and Dielectric Properties of Zinc Oxide Thin Films Obtained by Impedance Spectroscopy

H. Benattou*

Electronics Department, Laboratory of Elaboration and Characterizations of the Materials, Djillali Liabes University of Sidi Bel Abbes, Sidi Bel Abbes, Algeria

(Received 13 February 2026; revised manuscript received 20 October 2026; published online 28 October 2026)

Zinc Oxide thin films were successfully grown on glass substrates by the spray pyrolysis technique. The structural properties have been identified using X-ray diffraction spectra. The deposited films are of polycrystalline natures, they are of the compact hexagonal system. The optical properties were also studied using transmittance and reflectance measurements in the wavelength range of (200-2500 nm). Electrical impedance in complex form of thin films was measured in terms of frequency and temperature using HP4192 impedance meter. Semicircular arcs were obtained and were theoretically simulated to get the equivalent circuit parameters and to model the different processes taking place in the solid thin films. AC conductivity study expresses the behavior of disordered materials where the CBH (Correlated Barrier Hopping) model is the predominant. The complex permittivity obtained from electrical measurements reflects losses and dissipation of energy in thin films; and it attributed to the interfacial and dipolar polarization.

Keywords: Zinc oxide, Thin films, Impedance spectroscopy, Dielectric properties.

DOI: 10.21272/jnep.18(5).05013 PACS numbers: 73.50. – h, 73.63.Bd

1. INTRODUCTION

Zinc Oxide (ZnO) Chalcogenide is a material semiconductor, it is of the II-VI family of compounds [1], it has a larger gap of 3.2 eV to 3.39 eV [2-4] depending on the preparation method and doping rate. This allows it to have radiative transitions, and to have direct transitions between the valence band and the conduction band. ZnO has a hexagonal crystallographic structure of the type of wurtzite. Its refractive index is close to 2 when the material is in the massive form; when it is in thin films this index varies between 1.70 and 2.20. The absorption coefficient is equal to 10^4 cm^{-1}. ZnO in thin films has the particularity of being relatively transparent. It is used as window layers in solar Cells, and in author various applications [5, 6]. Doped zinc oxide is counted among the transparent conductive oxides (TCO). Very lightly doped, it can be used in luminescence. The main aim is to bring out the different properties of ZnO thin films elaborated by *t*he spray pyrolysis technique.

2. MATERIALS AND METHODS

2.1 Preparation of ZnO Layers

The starting product used is Zinc bichloride ($ZnCl_2$) with a molar mass of 136.315 g/mole; It is dissolved in distilled water. We have chosen molarity of 0.1 mol. The crystallization temperature of this material is 350 °C. The film thickness is measured a posteriori after the deposition. The thickness of the layer is a function of its mass and its surface, this is the weighing method for which the density of the material was used: (ρ_{ZnO} = 5.67 g·cm^{-3}) [7]. The properties extraction of ZnO thin films is done in several techniques: X-ray diffraction (XRD) to bring out structural properties. JASCO V-570 spectrophotometer operating in ultraviolet-visible – near-infrared spectral range (200-2500 nm) used for optical characterization. To bring out electrical and dielectric properties (impedance, conductivity, and permittivity) in alternating current measurements, we are used an HP 4192 impedance meter operating in the frequency range of 5 Hz-13 MHz. We are prepared our sample in coplanar configuration. ZnO material is a dielectric between two metal contacts.

3. RESULTS AND DISCUSSIONS

3.1 Structural Characterization by X-Ray Diffraction

The ZnO diffraction spectrum given in Fig. 1 is very rich in diffraction peaks, which means that the ZnO film produced is well crystallized. The most intense peak is that of (002) at 2θ = 34.6°. It is of the form of Miller's index of (00*l*) which proves that the crystallites grow with the $\vec{c}$ axis perpendicular to the substrate plane. We report the presence of other peaks on the same spectrum; they are also of significant intensity and which would be written in the form (*h*0*l*). All these peaks belong to ZnO of the compact hexagonal system.

ZnO crystal lattice parameters (*a*, *b*, and *c*) are those of hexagonal structure. It is done from the following quadratic relation, connecting the inter-reticular

* Correspondence e-mail: h.benattou@gmail.com

© 2026 The Author(s). Journal of Nano- and Electronic Physics published by Sumy State University. This article is distributed under the terms and conditions of the Creative Commons Attribution (CC BY) license.

Cite this article as: H. Benattou, *J. Nano- Electron. Phys.* 18 No 5, 05013 (2026) https://doi.org/10.21272/jnep.18(5).05013

distance (d_{hkl}) and the miller indices (hkl):

$$d_{hkl} = \frac{a}{\sqrt{\frac{4}{3}(h^2+k^2+hk)+l^2\frac{a^2}{c^2}}} \quad (1)$$

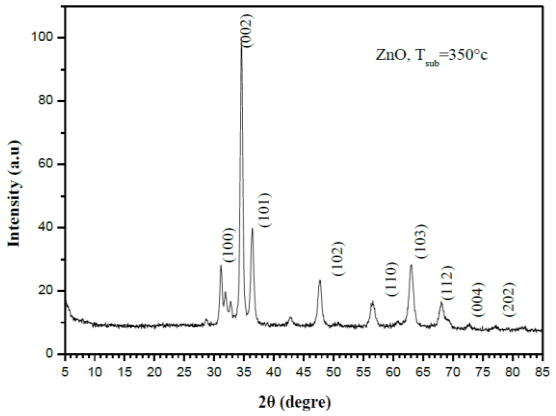


Fig. 1 – ZnO diffraction pattern

The calculated lattice parameters are: a = 3.246 Å, and c = 5.180 Å. They are in good agreement with the literature data [8-10].

In Fig. 2, we are used Lorentz fitting on the most intense peak (002) at the Bragg angle θ = 34.6° using following Scherrer formula [11]:

$$G = \frac{k \cdot \lambda}{W \cdot cos(\theta)} \quad (2)$$

Where W (in radian) is the Full-width half maximum of the most intense diffraction peak. To simplify the grains size (G) calculations, it is assumed that the grains have a spherical shape and we take a factor (k) value close to 1, the incident wavelength λ is 1.5406 Å. As a result, the grain size (G) was estimated to be around 198 Å (19.8 nm).

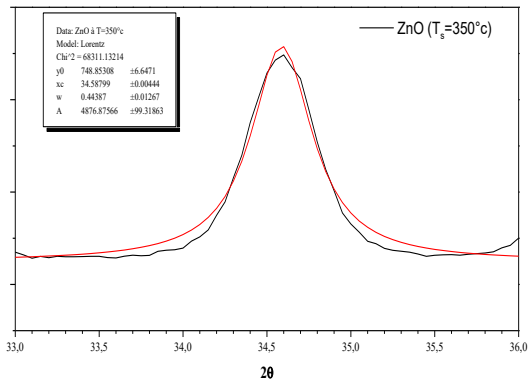


Fig. 2 – Lorentz fitting on ZnO diffraction diagram near the peak (002)

The stress "ε" thus calculated is a unitless quantity, which is proportional to the well-known structural stresses caused by the crystal lattice distortions [12]. Using the formulas (3), (4) and (5), the dislocation density (δ), the number of crystallites (N), and the value of the estimated stress (ε) are successive of the order of $2.55.10^{-3}$ lines per square nanometer, $6.9.10^{-2}$/nm^2, and $19.33 \cdot 10^{-4}$; (d) is the thickness of the thin film.

$$\delta = \frac{1}{G^2} \quad (3)$$

$$N = \frac{d}{G^3} \quad (4)$$

$$\varepsilon = \frac{W.cos\,\theta}{4} \quad (5)$$

3.2 Optical Characterization

In Fig. 3, we have plotted transmittance and reflectance spectra of the ZnO film as a function of the wavelength λ (in nm).

We can distinguish three areas. The first area below 375 nm wavelength: the Ultra Violet radiation range. The transmittance spectrum of ZnO layers weakens and then vanishes. This decrease corresponds to the fundamental absorption of thin-film material. The second region towards the variant wavelengths between 300 nm to 800 nm, where the transmittance increases abruptly, is the visible region that will be used for the determination of the optical absorption threshold; in this region, the transmittance does not exceed 70 %. The third region is in the near-infrared where the transmittance begins to increase quickly so that it roughly stabilizes at a value reached at 80 % up to 2500 nm. The reflectance of the layer reaches 10 % in the visible range. These results give ZnO thin films the transparency property.

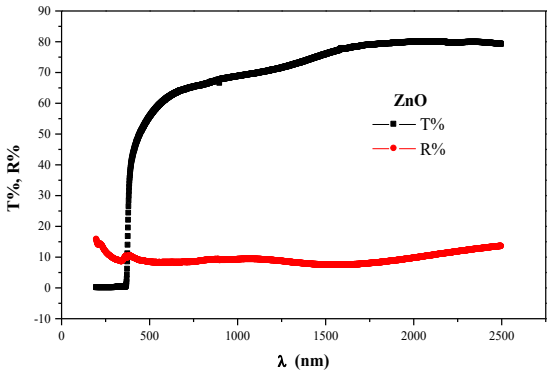


Fig. 3 – ZnO transmittance and reflectance spectra

The absorption coefficient α is expressed as the following formula: [13]

$$\alpha = \frac{1}{d}.Ln\left(\frac{1-R}{T}\right) \quad (6)$$

In Fig. 4, the shape of the absorption spectrum is as good as those of any semiconductor. We can see three regions. At low energies, the spectrum shows a residual absorption of the order of $1 \cdot 10^4$ cm^{-1} up to the photon energy of 3.2 eV, where we have the absorption of free carriers and phonons. A second region is that of the fundamental gap where an absorption front appears in the vicinity of 3.27 eV. It is characterized by a quadratic growth until the approach of the gap, that is to say, the direct transition of loads. The existence of an exciton peak around 3.25 eV is explained by the fineness of the ZnO particle's size and the exciton absorption. The third region is that strong absorption appears at energies greater than the optical gap (E_g). In Fig. 5, the curve $(\alpha h\nu)^2$ as a function of photon energy ($h\nu$) presents a linear part in the vicinity of the fundamental absorption threshold of which we can suggest that our ZnO films have a direct optical gap of the order of 3.27 eV.

Band tail width or Urbach energy (E_u) [14] estimated

in Fig. 6 represents the disorder in the film. It is of the order of 0.31 eV.

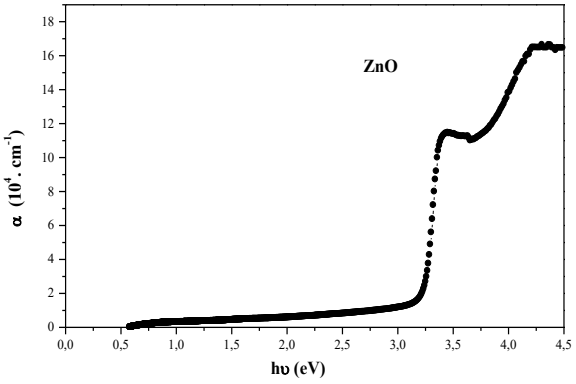


Fig. 4 – ZnO layer optical absorption spectrum

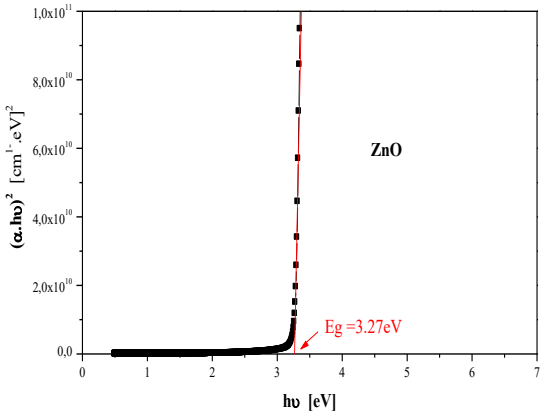


Fig. 5 – Optical gap of ZnO thin films

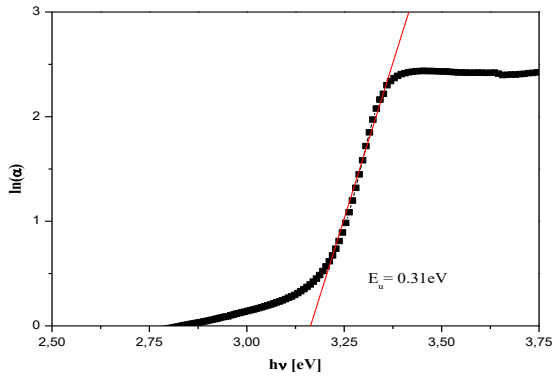


Fig. 6 – Urbach energy (E_u) in ZnO films

3.3 Electric and Dielectric Characterization

Complex impedance (Z^*) measurements in complex form (modulus (|Z|) and phase (θ)) are taken as a function of frequency and temperature. The result is interpreted in terms of a simple equivalent circuit consisting of a combination (series, parallel or mixed) of resistive and capacitive elements. By adjusting the curves, the numerical values of these elements are determined. Then, the conductivity and permittivity are determined according to the following formulas:

$$\sigma^* = \left(\frac{1}{\rho^*}\right) = \left(\frac{1}{Z^*}\right).\left(\frac{d}{S}\right) \qquad (7)$$

$$\varepsilon^* = 1/(i.\omega.C_0.Z^*) \qquad (8)$$

'S' is the electrode surface. ρ^* and ε^* are respectively resistivity, and permittivity in complex form. ω is the pulsation. C_0 is vacuum capacity. In Fig. 7 the Nyquist representation (Z'' vs Z') is in the form of two semicircles centered on the x-axis.

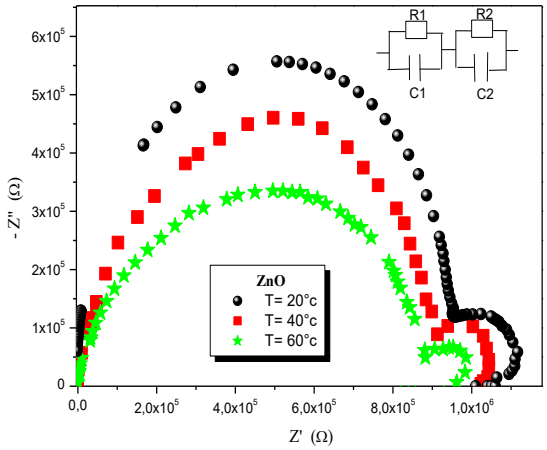


Fig. 7 – Nyquist representation (Z'' vs Z') of ZnO films

The first arc in low frequencies corresponds to the grain boundary contribution and the other in high frequencies corresponds to the grain contribution for electrical conduction [15]. Their diameters correspond to grain resistance value (R_g) at high frequencies, and grain boundary resistance (R_{gb}) at low frequencies. It is large at room temperature; it decreases with increasing temperature up to 40 °C and 60 °C. This is explained by a thermally activated process. The equivalent electrical circuit is that of a series of two circuits (R_1 C_1 and R_2 C_2) comprising a resistor chained in parallel with a capacitor. This model includes two relaxation times: $\tau_1 = R_1 \cdot C_1$ and $\tau_2 = R_2 \cdot C_2$, which can be calculated in Table 1.

Table 1 – The estimated relaxation time, resistances, and capacitors values

	T = 20 °C	T = 40 °C	T = 60 °C
τ_1 [μSec]	106	504.69	15932.5
τ_2 [μSec]	0.1592	20.044	63.34
R_1 [Ω]	944256.2	886189.94	881887.12
C_1 [Farad]	$1.956 \cdot 10^{-11}$	$2.1352 \cdot 10^{-11}$	$4.71 \cdot 10^{-11}$
R_2 [Ω]	174382.2	159188.7	11009.65
C_2 [Farad]	$1.154 \cdot 10^{-12}$	$4.0125 \cdot 10^{-11}$	$2.8942 \cdot 10^{-9}$

In the curves of Fig. 8 the two peaks reflect the contribution of grains and the grain boundaries and the existence of two relaxation times. The decrease seen in the real part at high frequency is reflected in the effect of reducing the material's ability to polarize (store energy) which corresponds to relaxation in the medium.

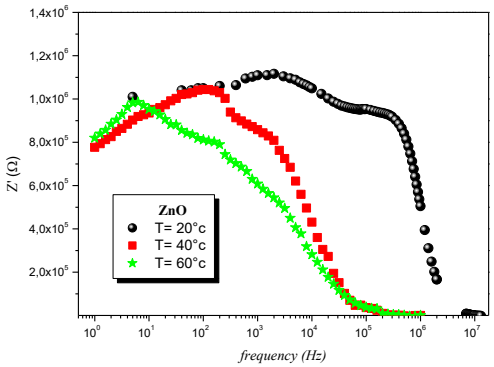


Fig. 8 – Z' vs frequency and temperature of ZnO thin films

In Fig. 9, the curve of Z'' vs frequency shows two temperatures. This indicates the presence of two relaxation processes; each characterized by a relaxation frequency which is written like the two following formulas:

$$f_1 = 1/(2\pi R_1 C_1) \quad (9)$$

$$f_2 = 1/(2\pi R_2 C_2) \quad (10)$$

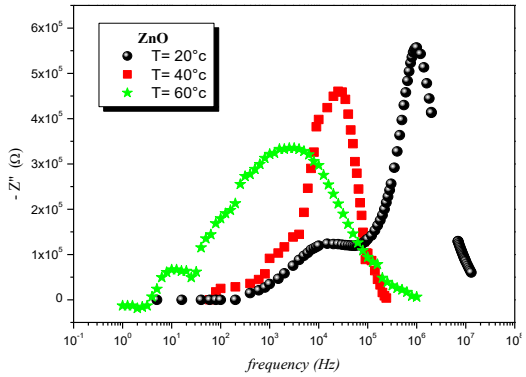


Fig. 9 – Z'' vs frequency and temperature of ZnO thin films

The relaxation times correspond to the relaxation frequencies for typical polarization mechanisms: orientation, interfacial or atomic.

In Fig. 10 the conductivity shape is independent of the frequency below a critical frequency (ω_c). In high frequency, the conductivity increases exponentially with the frequency according to the following empirical relation of Jonscher [16, 17], where the parameter "S" varies between (0 and 1).

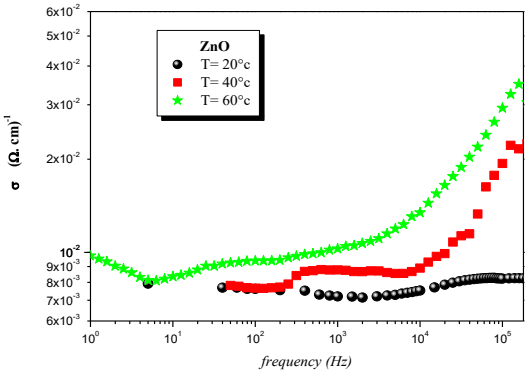


Fig. 10 – Electrical conductivity. vs frequency and temperature of ZnO films

This last mechanism takes its physical origin in the jumps between the site's pairs, randomly distributed.

$$\sigma_{AC}(\omega, T) = A(\omega, T).\omega^{s(\omega,T)} \quad (11)$$

The exponent 'S' depends on the temperature. It increases when the temperature increases, (see Table 2), this is suggested that the polaron tunnel model is the predominant AC conduction mechanism [17]. For this model, the exponent 'S' is written by the following relation:

$$S = 1 + \frac{4}{\frac{W_H}{k_B.T} + ln(\omega.\tau_{ph})} \quad (12)$$

The density of states at the Fermi level ($N(E_F)$) according to Austin and Mott theory [18] is written like the following formula:

$$\sigma(\omega) = \frac{\pi}{3}.e^2.k_B.T.N(E_F)^2.\alpha^{-5}.\omega.ln(\Omega/\omega)^4 \quad (13)$$

Where e is the loads, α is phonons vibration frequency, $\Omega = 5{\cdot}10^{12}$ Hz.

State density is defined as the number of free carriers per unit volume. It increases with temperature which agrees to a slight shift in the Fermi level.

Table 2 – The calculated values of the exponent, and state density at the Fermi level

	$T = 20$ °C	$T = 40$ °C	$T = 60$ °C
S	0.03859	0.33794	0.338362
N(EF)×10^{20} [$eV^{-1}{\cdot}cm^{-3}$]	0.83367	1.231	1.4602

In "Fig. 11", the increased values of the dielectric constant (ε') are interpreted by charge carriers' accumulation at the interface between the electrode and the solid. It is the predominant interfacial polarization phenomenon in the low and medium frequency range. Then, the ε' quantities are lowered due to migrations of charge carriers under the influence of the electric field. This is an orientation or dipolar phenomenon.

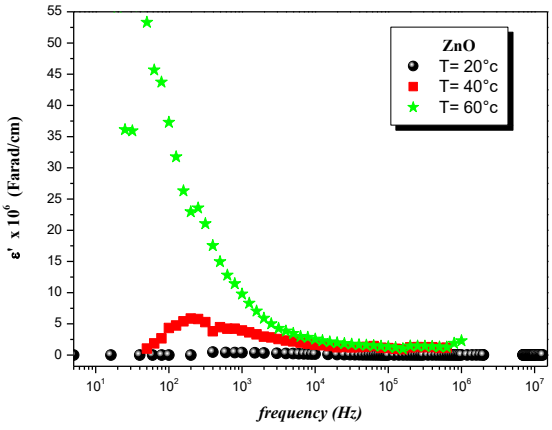


Fig. 11 – Dielectric constant (ε') vs frequency and temperature of ZnO thin films

In Fig. 12, the high values of (ε'') are attributed to the increased dielectric losses of nano-materials which are due to the increased defect structure at the grain boundaries. Temperature accelerates the charge carrier's conduction and facilitates the orientation of molecules.

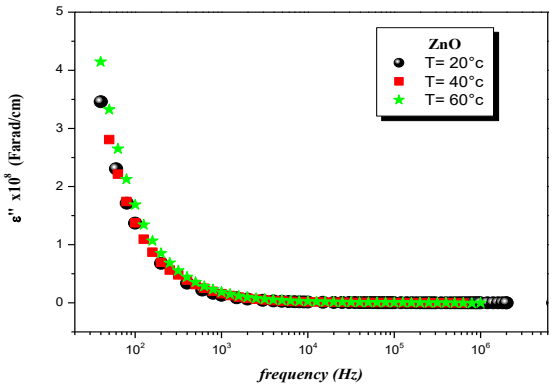


Fig.12 – Dielectric losses (ε''). vs frequency and temperature of ZnO thin films

4. CONCLUSION

ZnO thin films were prepared by the spray pyrolysis process. XRD indicates that the ZnO is embedded in the thin films in a compact hexagonal system with lattice parameters of a = 3.246 Å, c = 5.180 Å. The transmittance does not exceed 70 % in the visible region, and it increases to reach 80 % in the near-infrared region up to a wavelength of 2500 nm. ZnO films have a direct optical gap of the order of 3.27 eV. From impedance meter measurements, ZnO indicates that the polaron tunnel model is the predominant AC conduction mechanism. The interfacial polarization phenomenon in the low and medium frequency range is predominant; and orientation polarization phenomenon in the high frequencies.

REFERENCES

1. N.H. Kim, H.W. Kim, *Mater. Lett.* **58** No 6, 938 (2004) https://doi.org/10.1016/j.matlet.2003.07.040.
2. J. Zhu, D. Chakarov, M. Zäch, *Nanostructured Materials for Photolytic Hydrogen Production*, 441 (Ed. by L. Zang) *Energy Efficiency and Renewable Energy Through Nanotechnology, Green Energy and Technology* (Springer: London: 2011) https://doi.org/10.1007/978-0-85729-638-2_13.
3. H. Tabet-Derraz, N. Benramdane, D. Nacer, A. Bouzidi, M. Medles, *Sol. Energy Mater. Sol. C.* **73** No 3, 249 (2002) https://doi.org/10.1016/S0927-0248(01)00134-9.
4. B. Ergin, E. Ketenci, F. Atay, *Int. J. Hydrogen Energy* **34** No 12, 5249 (2009) https://doi.org/10.1016/j.ijhydene.2008.09.108.
5. N. Ito, Y. Sato, P.K. Song, A. Kaijio, K. Inoue, Y. Shigesato, *Thin Solid Films* **496** No 1, 99 (2006). https://doi.org/10.1016/j.tsf.2005.08.257.
6. J. Song, J. Park, H. Kim, Y.-W. Heo, J.-H. Lee, J.-J. Kim, *J. Electron. Mater.* **90** No 2, 022106 (2007) https://doi.org/10.1063/1.2430917.
7. A. Senol Aybek, N. Baysal, M. Zor, E. Turan, M. Kul, *Thin Solid Films* **515** No 24, 8709 (2007) https://doi.org/10.1016/j.tsf.2007.03.129.
8. G. Santana, A. Morales-Acevedo, O. Vigil, L. Vaillant, F. Cruz, G. Contreras-Puente, *Thin Solid Films* **373** No 1-2, 235 (2000) https://doi.org/10.1016/S0040-6090(00)01142-1.
9. N. Adhlakha, K.L. Yadav, A. Kumar, P.K. Patel, J. Rani, M. Rawat, *Physica B* **407** No 17, 3427 (2012) https://doi.org/10.1016/j.physb.2012.04.052.
10. F. Cruz-Gandarilla, A. Morales-Acevedo, O. Vigil, M. Hesiquio-Garduño, L. Vaillant, G. Contreras-Puente, *Mater. Chem. Phys.* **78** No 3, 840 (2003) https://doi.org/10.1016/S0254-0584(02)00395-4.
11. L. Alexander, H.P. Klug, *J. Appl. Phys.* **21** No 2, 137 (1950) https://doi.org/10.1063/1.1699612.
12. S. Prabahar, M. Dhanam, *J. Cryst. Growth* **285** No 1-2, 41 (2005) https://doi.org/10.1016/j.jcrysgro.2005.08.008.
13. H.A. Badran, M.F. Al-Mudhaffer, Q.M.A. Hassan, A.Y. Al-Ahmad, *Chalcogenide Lett.* **9** No 12, 483 (2012)
14. F. Urbach, *Phys. Rev.* **92** No 5, 1324 (1953) https://doi.org/10.1103/PhysRev.92.1324.
15. J. Ross, *Macdonald, Impedance Spectroscopy: Emphasizing Solid Materials and Systems* (Wiley-Interscience: New York: 1987).
16. A.K. Jonscher, *Nature* **267** No 5613, 673 (1977) https://doi.org/10.1038/267673a0.
17. A.R. Long, *Adv. Phys.* **31** No 5, 553 (1982) https://doi.org/10.1080/00018738200101418.
18. E.A. Davis, N.F. Mott, *Philos. Mag.* **22** No 179, 903 (1970) https://doi.org/10.1080/14786437008221061.

Структурні, оптичні та діелектричні властивості тонких плівок оксиду цинку, отримані методом імпедансної спектроскопії

H. Benattou

Electronics Department, Laboratory of Elaboration and Characterizations of the Materials, Djillali Liabes University of Sidi Bel Abbes, Sidi Bel Abbes, Algeria

Тонкі плівки оксиду цинку були успішно вирощені на скляних підкладках методом розпилювального піролізу. Структурні властивості були визначені за допомогою рентгенівських дифракційних спектрів. Осаджені плівки мають полікристалічний характер, вони мають компактну гексагональну систему. Оптичні властивості також були досліджені за допомогою вимірювань пропускання та відбиття в діапазоні довжин хвиль (200-2500 нм). Електричний імпеданс у складній формі тонких плівок вимірювався з точки зору частоти та температури за допомогою імпедансметра HP4192. Були отримані напівкруглі дуги, які були теоретично змодельовані для отримання параметрів еквівалентної схеми та моделювання різних процесів, що відбуваються в твердих тонких плівках. Дослідження провідності змінного струму відображає поведінку невпорядкованих матеріалів, де переважає модель КБС (корельованого бар'єрного стрибка). Комплексна діелектрична проникність, отримана з електричних вимірювань, відображає втрати та розсіювання енергії в тонких плівках; і це пояснюється міжфазною та диполярною поляризацією.

Ключові слова: Оксид цинку, Тонкі плівки, Імпедансна спектроскопія, Діелектричні властивості.